Chemical Vapor Deposition-Grown Graphene: The Thinnest Solid Lubricant

Kwang-Seop Kim,[†] Hee-Jung Lee,[†] Changgu Lee,[‡] Seoung-Ki Lee,[§] Houk Jang,[§] Jong-Hyun Ahn,[§] Jae-Hyun Kim,[†] and Hak-Joo Lee[†,*]

[†]Department of Nano Mechanics, Nano Convergence and Manufacturing Systems Research Division, Korea Institute of Machinery & Materials, 104 Sinseongno, Yuseong, Daejeon, 305-343, Republic of Korea, [‡]School of Mechanical Engineering, and [§]School of Advanced Materials Science & Engineering, SKKU Advanced Institute of Nanotechnology, Sungkyunkwan University, 300 Cheoncheon, Jangan, Suwon, Gyeonggi, 440-746, Republic of Korea

ABSTRACT As an atomically thin material with low surface energy, graphene is an excellent candidate for reducing adhesion and friction when coated on various surfaces. Here, we demonstrate the superior adhesion and frictional characteristics of graphene films which were grown on Cu and Ni metal catalysts by chemical vapor deposition and transferred onto the SiO_2/Si substrate. The graphene films effectively reduced the adhesion and friction forces, and multilayer graphene films that were a few nanometers thick had low coefficients of friction comparable to that of bulk graphite.

KEYWORDS: CVD-grown graphene · adhesion · friction · wear · thin solid lubricant

Since its discovery in 2004, graphene has drawn much attention in many research areas because of its exceptional properties, including very high mobility, superior mechanical strength, high thermal conductivity, and high optical transparency.[1−6] Graphene has shown promise for many potential applications, including organic solar cells, field-effect transistors, hydrogen storage, and ultracapacitors.[7] Graphene may be a good candidate for solid lubricants that reduce the adhesion and friction forces between contact surfaces on the micro- and nanoscale while protecting the coated surface. This is because graphene is atomically thin and strong, chemically stable even under severe environmental conditions, and stacked in a lamellar structure with low shear strength similar to graphite. Additionally, graphene surfaces are hydrophobic, indicating low surface energy,[8] and the surface energy can be easily tailored through simple surface treatment.[9] Recently, it was reported that pristine graphene sheets of more than four layers showed friction forces as small as that of bulk graphite,[10] and that graphene platelets added in oil increased the lubrication performance of oil.[11] These previous studies imply that graphene could be used effectively as a lubricant.

Interaction forces between contact surfaces, such as the adhesion and friction forces, are crucial in many applications at the nanoscale because of the high surface to volume ratio of nanomaterials and nanodevices.[12] The operation and lifetimes of microelectromechanical systems (MEMS) and nanoelectromechanical systems (NEMS) are dominated by interaction forces. In fabrication processes such as nanoimprint lithography and transfer printing, the adhesion between contact materials plays an important role in the fidelity of pattern formation. Various lubricant materials, micro-/nanopatterns, and surface treatment processes have been developed to control the interfacial forces between contacting surfaces. Recently, methods for synthesizing large-area graphene on metal layers through chemical vapor deposition (CVD) have been proposed, and graphene has been readily transferred onto various substrates.[13−17] CVD-grown graphene has great merit as a surface coating because of its excellent scalability and transferability. In this study, we characterized the adhesion and frictional properties of CVD-grown graphene to investigate the feasibility of graphene as a thin solid lubricant between contacting surfaces. We showed that CVD-grown graphene effectively reduced the adhesion and friction forces, and in particular, multilayer graphene grown on Ni (a few nanometers thick) had a low coefficient of friction comparable to that of bulk graphite.

RESULTS AND DISCUSSION

Graphene films with different numbers of layers were synthesized on Cu and Ni metal catalysts by CVD and transferred onto a SiO_2/Si substrate by a wet transfer method similar to a previously reported process.[16,17]

* Address correspondence to hjlee@kimm.re.kr.

Received for review March 29, 2011 and accepted May 5, 2011.

Published online May 05, 2011
10.1021/nn2011865

Monolayer graphene was grown on Cu foil and multilayer graphene (1−10 layers) was grown on a Ni layer deposited on the SiO_2/Si substrate. In this letter, the graphene grown on Cu (Ni) and then transferred onto a SiO_2/Si substrate by a wet transfer process is referred to as Cu (Ni)-grown graphene on SiO_2. Poly(methyl methacrylate) (PMMA) film was used as a supporting layer only in the transfer of Cu-grown graphene. Figure 1 shows optical and atomic force microscopy (AFM) images of Cu- and Ni-grown graphene transferred onto the SiO_2/Si substrate. Figure 1a shows that the Cu-grown graphene consisted primarily of a monolayer, and partial bi- or trilayer flakes were observed. The inset in Figure 1a shows the Raman spectra (Horiba HR800 with a laser wavelength of 514 nm, 50× objective lens) of graphene; typical G and 2D bands were observed at ~1580 and 2700 cm^{-1}, respectively. The ratio of 2D/G peaks was 2.0, indicating monolayer graphene.[18] Topography images (Figure 1c) revealed that the Cu-grown graphene was relatively flat, and the thickness of one layer of graphene was about 0.5 nm, a little thicker than the interlayer spacing in bulk graphite (0.34 nm).[19,20] Some fine PMMA residue and contaminants were observed on the graphene surface. The optical image of Ni-grown graphene shows clear contrast between areas with different numbers of graphene layers (Figure 1b). The Raman spectrum of graphene shows typical D, G, and 2D peaks for multilayer graphene. The AFM image of graphene (Figure 1d) shows that the surface was fairly rough with many peaks and valleys. The thickness variation on the graphene surface was a few nanometers, corresponding to a few tens of layers.

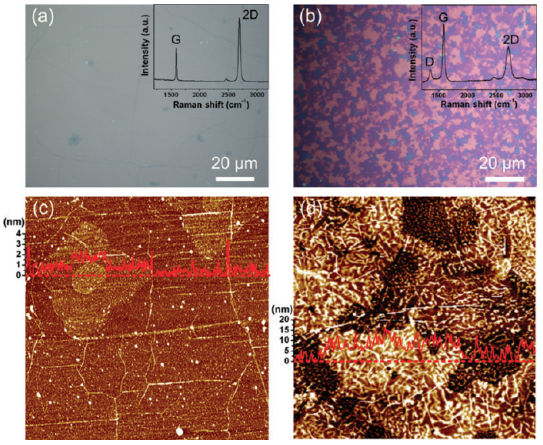

Figure 1. Optical (a, b) and AFM (c, d) images of Cu- and Ni-grown graphene transferred onto SiO_2/Si substrates: (a, c) optical and topography images of Cu-grown graphene on SiO_2; (b, d) optical and topography images of Ni-grown graphene on SiO_2. Insets in the optical image are Raman spectra for each graphene sample, showing the basic features of graphene. Insets in the AFM images are line profiles of position marked with a red dotted line. The AFM topography was obtained in noncontact mode, and the scan size was 10 μm × 10 μm.

The adhesion and friction tests were performed using a home-built microtribometer to investigate the adhesion and frictional characteristics of the graphene on the microscale. The adhesion tests were also conducted using a commercial AFM to interrogate the graphene samples on the nanoscale. Figure 2 shows the pull-off force on the graphene samples measured by the microtribometer and AFM. The results show that the pull-off force decreased due to the presence of the graphene films, and the effect of graphene on the pull-off force was influenced by the counterpart material in contact and the graphene samples. The counterpart materials were fused silica, representative of hard materials, and polydimethylsiloxane (PDMS), representative of soft materials. When the fused-silica lens was used as a counterpart material and the contact load was 10 mN, the pull-off force on bare SiO_2 was 12.4 mN and the pull-off forces on both Cu- and Ni-grown graphene were so small that the values were nearly equal to the measurement noise level (Figure 2a). When the contact load was increased to 50 mN, the pull-off forces were 0.25 mN on the Cu-grown graphene and 0.14 mN on the Ni-grown graphene, indicating that conformal contact between the fused-silica lens and the graphene did not occur under this contact load. Because the surface of the silica lens was

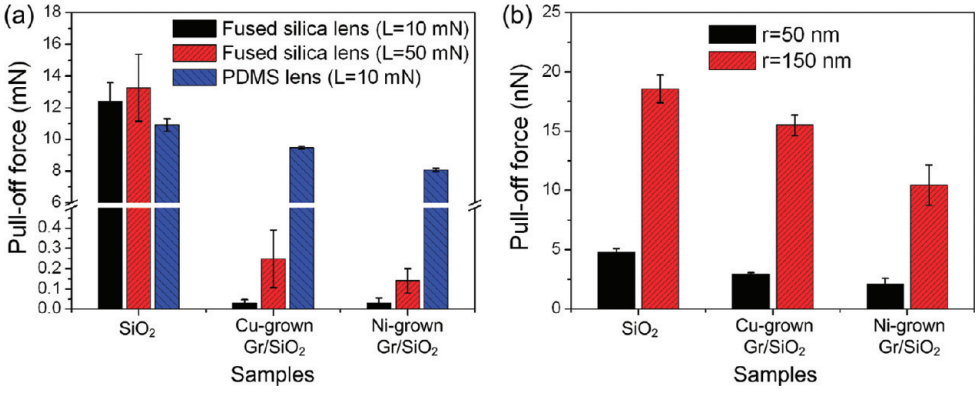

Figure 2. Pull-off force on graphene samples measured by (a) a microtribometer for microscale contact and (b) AFM for nanoscale contact. Gr: graphene.

stiff and hard, and residue, contaminant, and corrugation were present on the graphene surface due to synthesis and transfer processes, the real contact area between the lens and the graphene films was quite small, especially under small contact loads, and this resulted in low pull-off forces. For the PDMS lens, the conformal contact between the lens and the graphene films readily formed because PDMS is compliant, and its stiffness is several orders of magnitude lower than that of fused silica. The apparent contact radius between the PDMS lens and the graphene films was a few times larger than that between the fused-silica lens and the graphene films. The pull-off force on the Cu-grown graphene decreased about 13% compared with that on the bare SiO_2/Si substrate, and the pull-off force on the Ni-grown graphene decreased about 26% compared with that on the substrate. The water contact-angle measurements (Supporting Information, Figure S1) revealed that graphene had lower surface energy than SiO_2, resulting in a low adhesion force. The results on both graphene samples showed that when the graphene films contacted a hard material on the microscale, the surface contaminant and corrugation, rather than the surface energy, influenced adhesion between the graphene and the contact material, significantly decreasing adhesion. Therefore, it is suggested that a soft material, such as polymeric films, should be used as a substrate for conformal contact to increase adhesion between graphene and the substrate in applications requiring high adhesion or reliability. Interestingly, damage was not observed on graphene due to contact, even under repeated tests over three times at the same location on the sample. It was reported that the work of adhesion between graphite and the SiO_2 substrate was higher than the work of cohesion of graphite in the atomistic simulation based on density functional theory.[21] However, the transfer onto the fused silica lens of the CVD-grown graphene on the SiO_2 substrate was not observed in our experiment. The difference between the experimental results and the theoretical calculation could be due to the difference in contact geometry and the corrugation and contaminants present on the graphene surface. Also, there were similar variations in pull-off force among different graphene samples. That is, the pull-off force on Cu-grown graphene, which was thinner than Ni-grown graphene, was higher than that on Ni-grown graphene. This tendency was also observed in the nanoscale adhesion tests.

To investigate the adhesion properties of graphene during nanoscale contact, adhesion tests were performed by AFM to achieve single asperity contact and eliminate the effect of surface morphology on adhesion. Figure 2b shows the pull-off force measured by AFM on the same samples used in the microscale tests. During nanoscale contact, graphene also reduced the pull-off force, and changes in pull-off force with different graphene samples were similar to those in the microscale experiments using the PDMS lens, regardless of the tip radius. That is, the pull-off force on Cu-grown graphene was higher than that on Ni-grown graphene. The surface energy and pull-off force of graphene did not depend on the number of graphene layers in previous reports.[9,10] We believe that the higher pull-off force on Cu-grown graphene was due to residue from PMMA resist used as a supporting material for the wet transfer of the Cu-grown graphene. PMMA residue was not completely removed using conventional resist cleaning, similar to a previous report using scanning tunneling microscopy (STM).[20] In our graphene films, PMMA residue was present on the surface of the Cu-grown graphene, as shown later in the AFM image measured at the boundary of the wear track. The water contact angle was smaller on PMMA than on graphene (Supporting Information, Figure S1), indicating that the surface energy of PMMA is higher than that of graphene, increasing the pull-off force. The higher surface energy of PMMA is one of the reasons that the pull-off force on Cu-grown graphene was higher than that on Ni-grown graphene when conformal contact between the lens and graphene occurred. It seemed that damage or transfer of graphene onto the tip surface did not occur during repeated contact even under the maximum contact pressure of 2.0 GPa. The measured pull-off force was reproducible during three sets of tests.

In addition to its adhesion properties, a great concern is that CVD-grown graphene has lubricity despite its atomic-scale thickness when coated on a substrate. Recent studies on friction on atomically thin graphene revealed that graphene significantly lowers the friction between two surfaces when coated on solid surfaces at the nanoscale.[10,22] These reports suggest that graphene could be a promising lubricant, even on larger scales, because its mother material, graphite, has been widely used in dry lubrication applications.[23,24] In this context, we measured the friction forces on CVD-grown graphene during microscale contact.

Figure 3 shows the frictional characteristics of the graphene films. Graphene effectively reduced the friction force, and the coefficient of friction depended on the type of graphene film. The friction force on the SiO_2/Si substrate cleaned in piranha solution (a mixture of sulfuric acid and hydrogen peroxide in a 3:1 volume ratio)[25] before the friction test was quite high, corresponding to a coefficient of friction of 0.68. The friction force decreased markedly when graphene was transferred onto the substrate. The coefficient of friction was 0.22 for Cu-grown graphene on SiO_2 and 0.12 for Ni-grown graphene on SiO_2. Interestingly, Ni-grown graphene on SiO_2 had a lower coefficient of friction than Cu-grown graphene on SiO_2, and the coefficient of friction was close to that for bulk graphite on graphite sliding (0.1).[24] The friction force on the as-grown

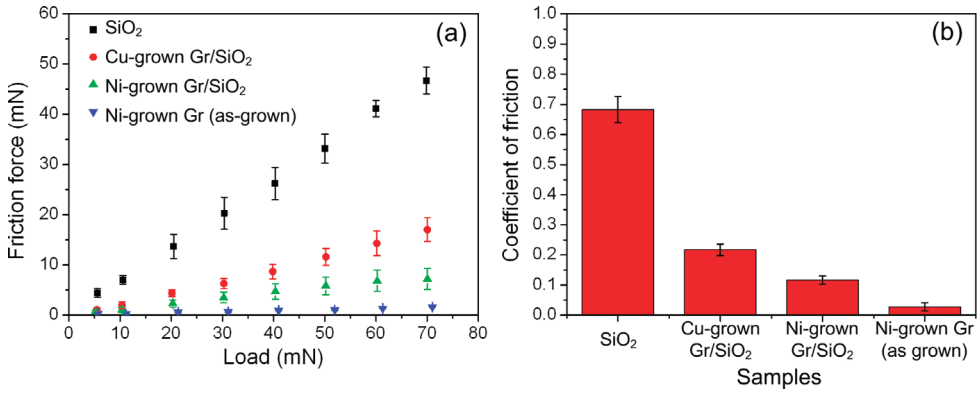

Figure 3. (a) Friction force as a function of load and (b) coefficient of friction for graphene samples. Only the fused-silica lens was used as a counterpart material in the friction tests. The coefficient of friction was calculated by dividing the friction force by the load in Figure 3a. The error bars in both graphs indicate standard deviation. Gr: graphene.

graphene on Ni decreased even more, and the coefficient of friction was about 0.03. The decrease in the real contact area between the fused-silica lens and the graphene, and the strong adhesion between the graphene and the underlying Ni layer resulted in the lowest coefficient of friction. The rough surface of the as-grown graphene resulting from the growth of Ni grains during high-temperature CVD decreased the real contact area between the fused-silica lens and graphene (Supporting Information, Figure S2a,b). Additionally, graphene was only slightly worn from the substrate and was not transferred onto the fused-silica lens surface, even after five test sets at the same location on the sample (Supporting Information, Figure S2c,d), indicating that the graphene was bonded tightly to the Ni layer. The friction measurement result for as-grown graphene on Ni revealed that the interaction between the graphene and the substrate is an important factor for friction, and suggests that strong adhesion of graphene to the surface not only reduces the surface friction significantly but also contributes to the wear reduction of the film and the surface. We recommend that the graphene–substrate interaction should be studied in depth to improve graphene films for surface coating.

To investigate the reason that Ni-grown graphene on SiO_2 had a lower coefficient of friction than Cu-grown graphene on SiO_2, we analyzed the wear track after the friction test using various surface analysis tools such as an optical microscope, AFM, Raman spectroscopy, and X-ray photoelectron spectroscopy (XPS). Figure 4 shows optical and AFM images of the wear track on the graphene samples after the friction tests. Cu-grown graphene on SiO_2 was partly worn due to the sliding, even in the first sliding, under a load of 5 mN in the first set of friction tests. In the next test where the load was 10 mN, the graphene was continuously worn along the sliding direction and the width of the wear track was narrow, but clearly shown. This result shows that adhesion between the graphene and the SiO_2 substrate was not strong. As the load increased to 70 mN in the first test set, the graphene was easily worn and the wear track became wider due to the increased contact area between the lens and the graphene. After that, two more sets of friction tests were performed at the same location on the sample, but the width of the wear track (~140 μm) changed little. After three sets of tests, the surface of the wear track was examined by optical microscopy (Figure 4a) and AFM. The AFM image of the center of the wear track (Figure 4b) shows that scratch lines formed along the sliding direction due to friction, and some wear debris was observed on the surface. The wear debris was primarily generated from the graphene worn from the substrate. At the boundary of the wear track (Figure 4c), part of the graphene remained because the contact pressure was almost zero at the proximate region between the lens and graphene. The line profile in Figure 4c shows that the remaining graphene was quite flat with a thickness of about 0.6 nm. The left side of the AFM image shows the region where contact between the lens and the graphene did not occur. There were many fine asperities on that region, and part of the PMMA residue remained on the graphene surface. The result also shows that rubbing under low contact pressure removed residue from the graphene. The graphene flakes worn during friction were mostly transferred onto the fused-silica lens, and the graphene film transferred onto the lens was a few tens of nanometers thick with many defects (Supporting Information, Figure S3). Therefore, after the fused silica lens slid against the Cu-grown graphene on SiO_2 a few times in the first set of friction tests, sliding occurred primarily between the SiO_2/Si substrate and the graphene films transferred onto the lens, as shown schematically in Figure 4d, resulting in a friction coefficient of 0.22.

Figure 4(e–h) shows observations of the wear track on Ni-grown graphene on SiO_2 after the friction tests. The thicker Ni-grown graphene on SiO_2 was more durable against sliding than the thinner Cu-grown graphene on SiO_2. In the first set of friction tests where the repeated tests with increasing load were performed

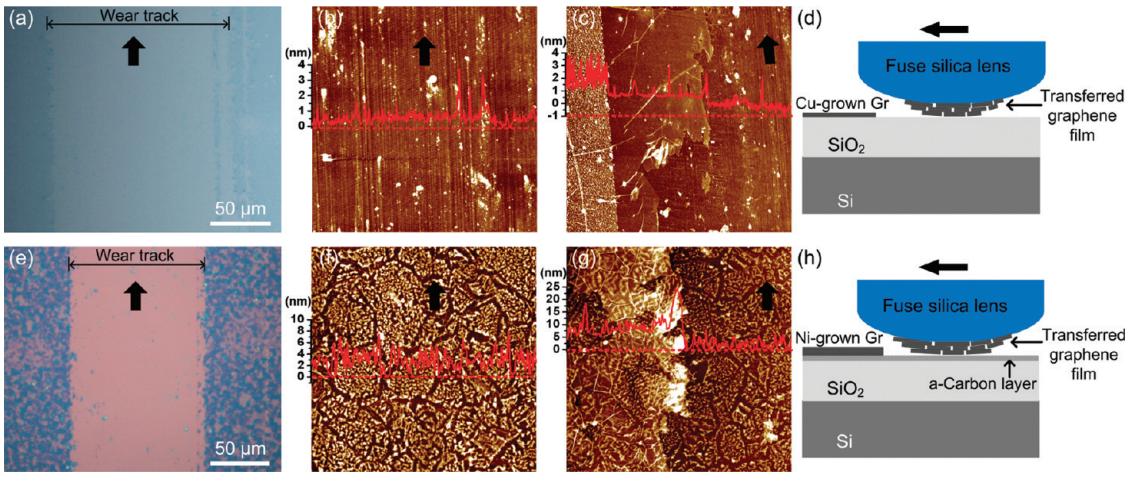

Figure 4. Optical and AFM images of the wear track on Cu-grown graphene (a−c) and Ni-grown graphene (e−g) after the friction tests, and an illustration of the rubbing surfaces in both cases (d, h). The black arrow in all optical and AFM images indicates the sliding direction of the fused-silica lens. (a) Optical image of the wear track on Cu-grown graphene. (b, c) AFM images at the center and boundary of the wear track. (d) Illustration of the rubbing surfaces during the friction tests for Cu-grown graphene. (e) Optical image of the wear track on Ni-grown graphene. (f, g) AFM images at the center and boundary of the wear track. (h) Illustration of the rubbing surfaces during the friction tests for Ni-grown graphene. AFM topography was obtained in noncontact mode, and the scan size was 10 μm × 10 μm. Line profiles marked as red dotted lines are shown on each topography image. Gr: graphene.

at the same location on the sample, the Ni-grown graphene was only partly worn up to a load of 50 mN. At a load of 70 mN, however, the graphene was almost worn out and the wear track was clearly visible. Four more sets of friction tests were performed at the same location on the sample, but the width of the wear track changed only slightly and some wear debris (a few micrometers in size) remained on the wear track as shown in Figure 4e. After that, the surface of the wear track was examined by AFM. Interestingly, in contrast to the Cu-grown graphene, the AFM image obtained at the center of the wear track (Figure 4f) showed that a thin layer patterned like a tortoise shell existed on the wear track. The layer surface was rough, and its thickness was in the range of 1−4 nm, as shown in the line profile. A thin layer with a tortoise shell-like pattern was also observed at the boundary of the wear track (right side of the AFM image in Figure 4g) along the sliding direction; the multilayer graphene film, not worn, is shown in the left side of the image. The thickness of the graphene films was in the range of 1−10 nm and varied significantly according to position. We believe that the thin layer with a tortoise shell-like pattern present on the wear track after the friction tests caused the differences in the frictional characteristics between the Cu- and Ni-grown graphene on SiO_2.

To investigate the layer with a tortoise shell-like pattern on the wear track of Ni-grown graphene, Raman and XPS spectra were obtained on the wear track of the graphene. The Raman spectrum on the nonworn region of Cu-grown graphene on SiO_2 shows typical graphene peaks, while the Raman spectrum on the center of the wear track shows that there was no graphene, indicating that graphene was worn out from the substrate (Figure 5a). The Raman spectrum of Ni grown graphene on SiO_2 (magenta line in Figure 5a), on the other hand, displayed weak, broad peaks in the range of 1200−1700 cm^{-1}, even on the wear track, indicating that amorphous carbon existed on the wear track of Ni-grown graphene.[26,27] XPS analysis also showed clearly that carbon existed on the wear track of Ni-grown graphene (magenta line in Figure 5b), and there were no other atoms, such as nickel and copper, used as catalysts except carbon, oxygen, and silicon. The oxygen and silicon peaks originated from the SiO_2 surface beneath the graphene. Thus, we believe that the layer with a tortoise shell-like pattern on the wear track was composed of amorphous carbon.

The relative amount of carbon on the sample surfaces was estimated quantitatively from the XPS spectra. The atomic concentration ratio of C 1s on Si 2p increases as the amount of carbon on SiO_2 increases. For Cu-grown graphene on SiO_2, the atomic concentration ratio of C 1s on Si 2p decreased from 2.0 on the nonworn region to 1.6 on the wear track of the graphene due to the wear. For Ni-grown graphene on SiO_2, the atomic concentration ratio decreased from 8.6 for the nonworn region to 3.3 for the wear track. The content of carbon on the wear track of the Ni-grown graphene was higher than that on the nonworn region of Cu-grown graphene, indicating that the amorphous carbon layer on the wear track of Ni-grown graphene was thicker than that on Cu-grown graphene, consistent with the AFM results.

According to the Raman and XPS analyses, the layer with a tortoise shell-like pattern on the wear track of

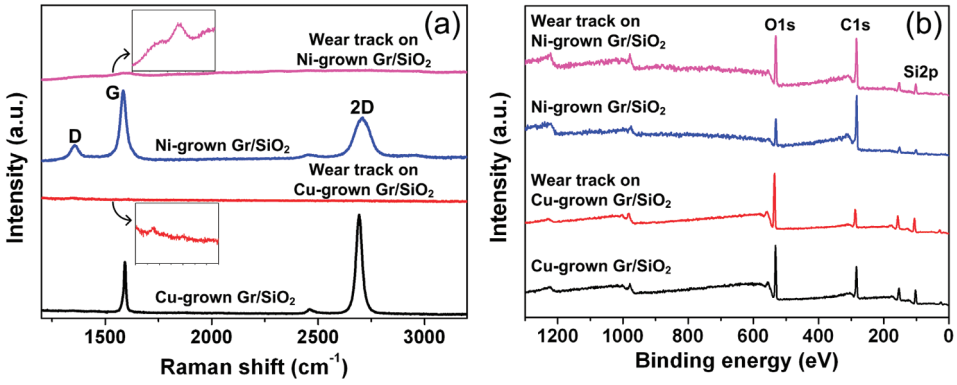

Figure 5. (a) Raman and (b) XPS spectra for graphene samples after the friction tests. The Raman spectra were obtained at a laser wavelength of 514 nm and a beam size of 1 μm. The insets in Figure 5a show magnified Raman spectra for the wear track in the range of 1200−1900 cm^{-1}. XPS spectra were obtained using a microfocused monochromator X-ray source with a beam size of 50 μm (Sigma Probe, Thermo Fisher Scientific, USA). Gr: graphene.

Ni-grown graphene was composed of amorphous carbon, not graphene, and the layer was thicker than the monolayer graphene. Although an amorphous carbon layer can be formed on a contact surface due to rubbing of carbon materials,[28,29] in this case it appeared that the amorphous carbon layer was not formed due to sliding but originated from the Ni-grown graphene. If the layer was a product of friction, it would also have been generated on the wear track of Cu-grown graphene. The layer could have been generated from carbon atoms that were segregated on the Ni surface during graphene synthesis, but did not form perfect sp2 bonding during CVD.[30,31] Therefore, repeated sliding during the friction tests for Ni-grown graphene caused the graphene film transferred onto the fused-silica lens to slide against the amorphous carbon layer adhered to the SiO_2/Si substrate, as shown schematically in Figure 4h, decreasing the friction coefficient to 0.12. The coefficient of friction was comparable to that for graphite-to-graphite sliding where an amorphous carbon layer can be generated at the interface due to friction. The results showed that the amorphous carbon layer underlying the multilayer graphene grown on Ni significantly affected the tribological characteristics of the graphene. Additionally, it is expected that Ni-grown graphene should be more durable and have a longer wear lifetime due to the contribution from the amorphous carbon layer adhered strongly to the SiO_2/Si substrate.

CONCLUSIONS

In summary, we measured the adhesion and friction forces on graphene films synthesized by CVD and transferred onto a SiO_2/Si substrate, and observed reduced adhesion and friction during micro- and nanoscale contact. The low surface energy of graphene and the topological surface modification by contaminants or wrinkles due to the transfer contributed to the low adhesion of graphene-coated surfaces. CVD-grown graphene also reduced the surface friction significantly, similar to the effects of graphite in many conventional applications. Ni-grown graphene on SiO_2 was relatively durable and had a low friction coefficient compared with Cu-grown graphene on SiO_2, resulting from the amorphous carbon layer with many defects, and a tortoise shell-like pattern. Ni-grown graphene had a coefficient of friction comparable to that of bulk graphite, indicating that graphene that is a few nanometers thick is a potential solid lubricant at the micro- and nanoscale. Additionally, the as-grown graphene on Ni showed the lowest coefficient of friction (0.03), and the frictional and wear characteristics of the multilayer graphene improved when the graphene was bonded tightly to the substrate and had nanoscale variations in thickness on the surface. The CVD-grown graphene films exhibited a strong potential for reducing the adhesion and friction forces and protecting the substrate surface.

METHODS

Preparation of Graphene Samples. Monolayer graphene was synthesized on Cu foil (25 μm thick) by chemical vapor deposition (CVD) in a 4-in. quartz tube.[17] While the furnace was heated to 1000 °C, H_2 (8 sccm) gas flow cleaned and reduced the Cu catalyst. CH_4 (24 sccm) flowed for 30 min to generate a carbon source at 1000 °C. Then, all input gases and power, except for H_2, were turned off, and the furnace was cooled to below 100 °C. After graphene synthesis, poly(methyl methacrylate) (PMMA) was coated on one side of the Cu foil to protect the synthesized graphene during the etching process of graphene placed on the opposite side of the foil. The Cu catalyst was removed by 0.1 M ammonium persulfate solution, $(NH_4)_2S_2O_8$, for 5 h, followed by rinsing with deionized (DI) water. After the PMMA-coated graphene was transferred onto the target substrate, the PMMA supporter was removed by dipping the sample in acetone at 80 °C to minimize the PMMA residue.

Multilayer graphene was synthesized on a Ni metal catalyst deposited onto a SiO_2/Si substrate.[16] The sample was heated to

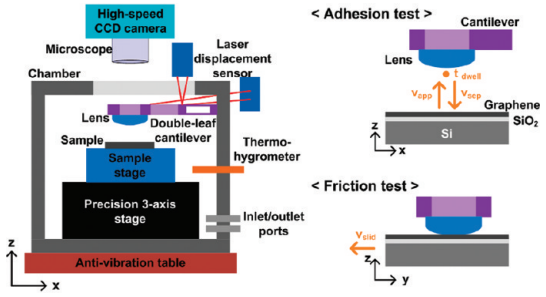

Figure 6. Schematic diagram of the microtribometer and test procedure.

TABLE 1. Experimental Conditions for the Adhesion and Friction Tests Using a Microtribometer

Adhesion Test	
lens (radius of curvature, R (mm))	PDMS (10.3), fused silica (25.8)
approach speed, v_{app} (μm/s)	10
max. applied load, L (mN)	10
max. contact pressure* (MPa)	0.05 (PDMS), 19 (fused silica)
dwell time, t_{dwell} (s)	5
separation speed, v_{sep} (μm/s)	5
Friction Test	
lens (radius of curvature, R (mm))	fused silica (25.8)
applied load (mN)	5—70
max. contact pressure* (MPa)	15—37
sliding distance (μm)	1000
sliding speed, v_{slid} (μm/s)	50

* The maximum contact pressure was calculated using Hertz's contact theory[32] under the given load. The elastic modulus and Poisson's ratio used in the calculation are 73 GPa and 0.17 for the fused silica lens, 2 MPa and 0.48 for the PDMS lens, and 130 GPa and 0.28 for the Si(100) substrate.

1000 °C in Ar (1000 sccm) without H_2 flow. After heating, the Ni catalyst was annealed for 25 min in Ar with flowing H_2 (250 sccm). After injecting the carbon source using CH_4 (150 sccm) for 7 s, the chamber was cooled rapidly to synthesize the graphene. Because the multilayer graphene did not need a supporting layer, Ni/graphene was floated on buffered oxide etchant (BOE) by removing the underlying SiO_2 layer. The Ni catalyst was removed using 1 M ferric chloride solution, $FeCl_3$, for 10 min followed by rinsing with DI water. Then, the multilayer graphene was transferred onto a SiO_2/Si substrate.

Adhesion and Friction Tests. For the adhesion and friction tests on the graphene films, a laser-quality fused-silica plano-convex lens (PLCX-10.0-25.8-UV, CVI Melles Griot, Albuquerque, NM, USA) and a polydimethylsiloxane (PDMS, Sylgard 184, Dow Corning, Midland, MI, USA) lens were used as the counterpart material. The radius of curvature of the fused-silica lens was 25.8 mm. The fused-silica lens was cleaned in piranha solution before adhesion and friction tests. The PDMS lens was fabricated by a molding method. After a mixture of degassed prepolymer and initiator (10:1) was prepared, it was poured onto a fused-silica mold with a radius of curvature of 10.3 mm and then cured in an oven overnight at 75 °C. The cured PDMS was readily detached from the lens without a release agent.

The adhesion and friction forces between the lens and the graphene films were measured using a home-built microtribometer. Figure 6 shows schematic diagrams of the microtribometer and test procedure. The microtribometer was installed in a chamber where the ambient conditions of relative humidity and gas could be controlled. A double-leaf cantilever was used to measure the pull-off and friction forces, which were determined from the deflection of the cantilever measured using laser-displacement sensors aligned in the direction of the y- and z-axes. To measure the force applied to the cantilever quantitatively, the force was calibrated against the sensor output, which was determined by adding and then removing weights one at a time. The force resolution of the system was 0.02 mN.

TABLE 2. Experimental Conditions for the Adhesion Tests Using an Atomic Force Microscope

Adhesion Test	
tip (radius of curvature, r (nm)/stiffness of the cantilever, k (N/m))	HD-DLC tip (50/0.2, 150/2.8)
approach speed, v_{app} (nm/s)	30
max. applied load, L (nN)	10—20
max. contact pressure* (GPa)	1.6—2.0 (r = 50 nm) 0.95—0.75 (r = 150 nm)
dwell time, t_{dwell} (s)	3
separation speed, v_{sep} (nm/s)	30

* The maximum contact pressure was calculated using Hertz's contact theory[32] under the given load. The elastic modulus and Poisson's ratio are 800 GPa and 0.14 for the HD-DLC tip and 75 GPa and 0.17 for the SiO_2 substrate.

For the adhesion tests, the graphene sample was moved upward to contact the lens by moving the z-axis stage. The sample was pressed against the lens until the load reached the predetermined maximum applied load, and contact was maintained for a dwell time. Then, the sample was separated from the lens at a constant unloading velocity by lowering the z-axis stage. The pull-off force was determined from the measured force data and defined as the maximum adhesion force during the unloading segment. The adhesion test was repeated more than three times at the same location of the sample, and the repeated tests were conducted at more than three different locations on each sample.

For the friction tests, after the sample contacted the lens under a constant contact load, the sample stage was moved along the y-direction, and the lens slid against the sample. The cantilever was deformed in the y-direction due to the friction force, which was a time-averaged value of force along the y-axis during steady-state sliding. The coefficient of friction was calculated by dividing the friction force by the load. Only the fused-silica lens was used as a counterpart material for the friction tests. For each set of friction tests, the replicate tests were performed at the same location as the load increased from 5 to 70 mN. Each set was repeated more than three times, usually five times, on the same location of the substrate. The data set was collected for different locations on the sample. The temperature and relative humidity in the chamber were measured using a thermohygrometer. During the experiments, the relative humidity and temperature of the chamber were 33 $\pm$ 3% and 21 $\pm$ 1 °C, respectively. The contact area between the lens and the graphene films during the tests was observed in real time using a microscope and high-speed charge-coupled device (CCD) camera module above the cantilever. Images were recorded simultaneously and analyzed later. The test conditions are presented in Table 1.

An atomic force microscope (XE-100, Park Systems, Korea) was used to investigate the adhesion properties of the graphene films during nanoscale contact. In the nanoscale adhesion tests, the topography effect on the measured adhesion force was negligible compared with that in the microscale tests. A high-density, diamond-like carbon (HD-DLC) probe (Nanotools, Germany) was used because it offered a hemispherical, symmetric, hydrophobic, smooth, and hard tip, providing a consistent pull-off force due to the robustness of the tip against multiple contacts. Two probes with different tip radii and cantilever stiffness were used. The tip radius and cantilever stiffness provided by the manufacturer was used. Using the probes, an adhesion test was conducted on bare SiO_2 as a reference substrate and the Cu-grown graphene films were tested. Then, a test was conducted on bare SiO_2 again, and the Ni-grown

graphene was tested. This procedure was repeated more than three times, and the tests on each sample were conducted more than three times at different locations. The test conditions are presented in Table 2. During the experiments, the relative humidity and temperature were 30 ± 3% and 20 ± 1 °C, respectively.

Acknowledgment. This research was supported by a grant (2009K000179) from the Center for Nanoscale Mechatronics & Manufacturing, one of the 21st Century Frontier Research Programs supported by the Ministry of Education, Science, and Technology, and by National Platform Technology Project supported by the Ministry of Knowledge Economy, Republic of Korea. The research was also partially supported by Basic Science Research Program (2010-0015035) through the National Research Foundation of Korea (NRF) funded by the Ministry of Education, Science and Technology, Republic of Korea.

Supporting Information Available: Water contact angle data, optical and AFM images of the wear track on as-grown graphene samples, and surface analysis data of the graphene film transferred onto the fused-silica lens after the friction tests. This material is available free of charge *via* the Internet at http://pubs.acs.org.

REFERENCES AND NOTES

1. Novoselov, K. S.; Geim, A. K.; Morozov, S. V.; Jiang, D.; Zhang, Y.; Dubonos, S. V.; Grigorieva, I. V.; Firsov, A. A. Electric Field Effect in Atomically Thin Carbon Films. *Science* **2004**, *306*, 666–669.
2. Novoselov, K. S.; Geim, A. K.; Morozov, S. V.; Jiang, D.; Katsnelson, M. I.; Grigorieva, I. V.; Dubonos, S. V.; Firsov, A. A. Two-Dimensional Gas of Massless Dirac Fermions in Graphene. *Nature* **2005**, *438*, 197–200.
3. Zhang, Y.; Tan, J. W.; Stormer, H. L.; Kim, P. Experimental Observation of the Quantum Hall Effect and Berry's Phase in Graphene. *Nature* **2005**, *438*, 201–204.
4. Wang, X.; Zhi, L.; Müllen, K. Transparent, Conductive Graphene Electrodes for Dye-Sensitized Solar Cells. *Nano Lett* **2008**, *8*, 323–327.
5. Lee, C.; Wei, X.; Kysar, J. W.; Hone, J. Measurement of the Elastic Properties and Intrinsic Strength of Monolayer Graphene. *Science* **2008**, *321*, 385–388.
6. Balandin, A. A.; Ghosh, S.; Bao, W.; Calizo, I.; Teweldebrhan, D.; Miao, F.; Lau, C. N. Superior Thermal Conductivity of Single-Layer Graphene. *Nano Lett.* **2008**, *8*, 902–907.
7. Zhu, Y.; Murali, S.; Cai, W.; Li, X.; Suk, J. W.; Potts, J. R.; Ruoff, R. S. Graphene and Graphene Oxide: Synthesis, Properties, and Applications. *Adv. Mater.* **2010**, *22*, 3906–3924.
8. Wang, S.; Zhang, Y.; Abidi, N.; Cabrales, L. Wettability and Surface Free Energy of Graphene Films. *Langmuir* **2009**, *25*, 11078–11081.
9. Shin, Y. J.; Wang, Y.; Huang, H.; Kalon, G.; Wee, A. T. S.; Shen, Z.; Bhatia, C. S.; Yang, H. Surface-Energy Engineering of Graphene. *Langmuir* **2010**, *26*, 3798–3802.
10. Lee, C.; Li, Q.; Kalb, W.; Liu, X.-Z.; Berger, H.; Carpick, R. W.; Hone, J. Frictional Characteristics of Atomically Thin Sheets. *Science* **2010**, *328*, 76–80.
11. Lin, J.; Wang, L.; Chen, G. Modification of Graphene Platelets and Their Tribological Properties as a Lubricant Additive. *Tribol. Lett.* **2011**, *41*, 209–215.
12. Bhushan., B., Micro/Nanotribology of MEMS/NEMS Materials and Devices. In *Nanotribology and Nanomechanics: An Introduction*; Bhushan., B., Eds.; Springer Verlag: Berlin, 2005; pp 1031−1083.
13. Yu, Q.; Lian, J.; Siriponglert, S; Hao, L; Yong, P. C.; Shin-Shem, P. Graphene Segregated on Ni Surfaces and Transferred to Insulators. *Appl. Phys. Lett.* **2008**, *93*, 113103.
14. Reina, A.; Jia, X.; Ho, J.; Nezich, D.; Son, H.; Bulovic, V.; Dresselhaus, M. S.; Kong, J. Large Area, Few-Layer Graphene Films on Arbitrary Substrates by Chemical Vapor Deposition. *Nano Lett.* **2009**, *9*, 30–35.
15. Li, X.; Cai, W.; An, J.; Kim, S.; Nah, J.; Yang, D.; Piner, R.; Velamakanni, A.; Jung, I.; Tutuc, E.; *et al.* Large-Area Synthesis of High-Quality and Uniform Graphene Films on Copper Foils. *Science* **2009**, *324*, 1312–1314.
16. Kim, K. S.; Zhao, Y.; Jang, H.; Lee, S. Y.; Kim, J. M.; Kim, K. S.; Ahn, J. H.; Kim, P.; Choi, J. Y.; Hong, B. H. Large-Scale Pattern Growth of Graphene Films for Stretchable Transparent Electrodes. *Nature* **2009**, *457*, 706–710.
17. Bae, S.; Kim, H.; Lee, Y.; Xu, X.; Park, J - S.; Zheng, Y.; Balakrishnan, J.; Lei, T.; Kim, H. R.; Song, Y. I.; *et al.* Roll-to-Roll Production of 30-Inch Graphene Films for Transparent Electrodes. *Nat. Nanotechnol.* **2010**, *5*, 574–578.
18. Ferrari, A. C.; Meyer, J. C.; Scardaci, V.; Casiraghi, C.; Lazzeri, M.; Mauri, F.; Piscanec, S.; Jiang, D.; Novoselov, K. S.; Roth, S.; *et al.* Raman Spectrum of Graphene and Graphene Layers. *Phys. Rev. Lett.* **2006**, *97*, 187401.
19. Novoselov, K. S.; Jiang, D.; Schedin, F.; Booth, T. J.; Khotkevich, V. V.; Morozov, S. V.; Geim, A. K. Two-Dimensional Atomic Crystals. *Proc. Natl. Acad. Sci. U.S.A.* **2005**, *102*, 10451–10453.
20. Ishigami, M.; Chen, J. H.; Cullen, W. G.; Fuhrer, M. S.; Williams, E. D. Atomic Structure of Graphene on SiO_2. *Nano Lett.* **2007**, *7*, 1643–1648.
21. Li, D.; Windl., W.; Padture, N. P. Toward Site-Specific Stamping of Graphene. *Adv. Mater.* **2009**, *21*, 1243–1246.
22. Filleter, T.; McChesney, J. L.; Bostwick, A.; Rotenberg, E.; Emtsev, K. V.; Seyller, Th.; Horn, K.; Bennewitz, R. Friction and Dissipation in Epitaxial Graphene Films. *Phys. Rev. Lett.* **2009**, *102*, 086102.
23. Erdemir, A.; Donnet, C. Solid Lubricants and Self-Lubricating Films. In *Modern Tribology Handbook*; Bhushan, B., Eds.; CRC Press: New York, 2001; pp 799−802.
24. Bowden, F. P.; Tabor, D. *The Friction and Lubrication of Solids Part II*; Clarendon press: Oxford, 1964; pp 186−193.
25. CAUTION: piranha solution is hazardous and can cause explosions or severe skin burns if not handled with great care.
26. Scheibe, H.-J.; Drescher, D.; Alers, P. Raman Characterization of Amorphous Carbon Films. *Fresenius J. Anal. Chem.* **1995**, *353*, 695–697.
27. Zheng, M.; Takei, K.; Hsia, B.; Fang, H.; Zhang, X.; Ferralis, N.; Ko, H.; Chueh, Y. -L.; Zhang, Y.; Maboudian, R.; *et al.* Metal-Catalyzed Crystallization of Amorphous Carbon to Graphene. *Appl. Phys. Lett.* **2010**, *96*, 063110.
28. Erdemir, A.; Donnet, C. Tribology of Diamond-Like Carbon Films: Recent Progress and Future Prospects. *J. Phys. D: Appl. Phys.* **2006**, *39*, R311–327.
29. Pastewka, L.; Moser, S.; Gumbsch, P.; Moseler, M. Anisotropic Mechanical Amorphization Drives Wear in Diamond. *Nat. Mater.* **2011**, *10*, 34–38.
30. Wintterlin, J.; Bocquet, M. −L. Graphene on Metal Surfaces. *Surf. Sci.* **2009**, *603*, 1841–1852.
31. Kahng, Y. H.; Lee, S.; Choe, M.; Jo, G.; Park, W.; Yoon, J.; Hong, W. K.; Cho, C. H.; Lee, B. H.; Lee, T. A Study of Graphene Films Synthesized on Nickel Substrates: Existence and Origin of Small-Base-Area Peaks. *Nanotechnology* **2011**, *22*, 045706.
32. Johnson, K. L. *Contact Mechanics*; Cambridge University Press: Cambridge, 1985; pp 84−106.